Guidance Logic for Spiral Approaches

Walter M. Hollister*
Massachusetts Institute of Technology, Cambridge, Mass.
and
William C. Hoffman†
Aerospace Systems, Inc., Burlington, Mass.

A spiral approach concept is proposed as a standard procedure for independent, commercial VTOL operations conducted in close proximity to CTOL operations. A guidance logic is developed for this VTOL application, although the results may be applicable to curved approaches by STOL or CTOL aircraft as well. The guidance concept attempts to maintain constant airspeed along a fixed-radius nominal spiral. The presence of wind requires a continuous variation in bank angle and heading rate to remain on the desired path. Linear perturbation analysis is used to select satisfactory feedback gains for commanded bank angle, longitudinal acceleration, and vertical speed. A wind estimator detects differences between the predicted and observed wind and uses the result to modify the nominal control. For four-dimensional (4-D) guidance, the nominal time must be computed as a function of turn angle, which requires the solution of an elliptic integral. Time-varying longitudinal accelerations are necessary for 4-D guidance when the observed wind differs from the predicted wind or when wind shear is present. The logic and the linear feedback gains have been tested in a nonlinear simulation. Results generally have verified the performance predicted by linear analysis.

Nomenclature

a	= longitudinal acceleration, ft/sec^2
g	= acceleration of gravity, 32.17 ft/sec^2
h	= altitude, ft
p	= $d/d\theta$ = Laplace operator in angle domain, 1/rad
r	= radial distance from spiral center, ft
t	= time, sec
u	= control vector
x	= state vector
$C_{(\,)}, K_{(\,)}$	= guidance gains
F	= linearized system dynamics matrix
G	= linearized system control matrix
V	= airspeed, fps
V_g	= ground speed, fps
W	= wind magnitude, fps
W_t, W_r	= tangential and radial wind components, fps
η	= wind direction, rad
θ	= azimuth angle around spiral from North, rad
θ_c	= characteristic angle for wind estimator, rad
ψ	= heading angle, rad
ϕ	= bank angle, rad
$(\,)_c$	= commanded value
$(\,)_f$	= value at spiral exit
$(\,)_0$	= value at spiral entry
$(\,)^*$	= nominal spiral value
$(\hat{\ })$	= navigation system estimate

Introduction

THE achievement of efficient all-weather VTOL commercial service to conventional airports requires that VTOL aircraft be operated essentially independent of existing CTOL aircraft route structures and procedures. The establishment of such independent VTOL operations during the takeoff and landing phases must take into account noise restrictions, obstacle clearance, VTOL aircraft performance capabilities, and interaction with CTOL air traffic. Previous studies of navigation and guidance requirements for VTOL operations at CTOL airports[1] have suggested the use of spiral descents by VTOL aircraft as a means of achieving efficient, safe operations that are independent of CTOL aircraft route structures and procedures.

At the present time, instrument flight rules (IFR) operations of CTOL aircraft create a wall of airspace along the active runway which is typically 10 miles long, 1500 ft high, and some hundreds of feet wide. The protected airspace is utilized by CTOL aircraft making instrument landing system (ILS) approaches, departures, and missed approaches; it creates a problem for VTOL traffic desiring to cross the active runway with no interference to the CTOL traffic flow. A suggested noninterfering VTOL approach to a conventional airport is illustrated in Fig. 1. Under this concept, the airspace directly over the active runway is partitioned such that the VTOL traffic has free access to cross over the runway perpendicular to the CTOL traffic at 1000 ft automatic gain control (AGL). Failure to allow IFR crossing of the CTOL runway in this way would necessitate an approach capability to both sides of each CTOL IFR approach course, followed by an air taxi across active runways. Such operations across active runways would have to be conducted under CTOL air traffic control, which could cause excessive delays and would make the VTOL traffic dependent on the CTOL operations.

After the 1000-ft crossing, the VTOL will take 2 min to descend at a rate of 500 ft/min. To expedite the approach, it is desirable to begin the turn to the pad as soon as possible. Using a standard turn rate (3 deg/sec) at an airspeed of 60 knots, the approach will consist of a spiral descent with turn radius of about 2000 ft, which fits conveniently into the typically available airspace. This solution has the advantage of keeping the two traffic flows independent and without mutual interference.

The spiral descent retains most of the advantages of a vertical descent but requires less power, maintains forward airspeed and controllability, and avoids the vortex ring state. The problem with the spiral descent operation is that it

Presented as Paper 76-1959 at the AIAA Guidance and Control Conference, San Diego, Calif., Aug. 16-18, 1976 (in bound volume of Conference papers); submitted Sept. 20, 1976; revision received April 27, 1977.

Index categories: Civil Missions and Transportation; Guidance and Control; Helicopters.

*Professor of Aeronautics and Astronautics; also Consultant to Aerospace Systems, Inc. Associate Fellow AIAA.

†Senior Project Engineer.

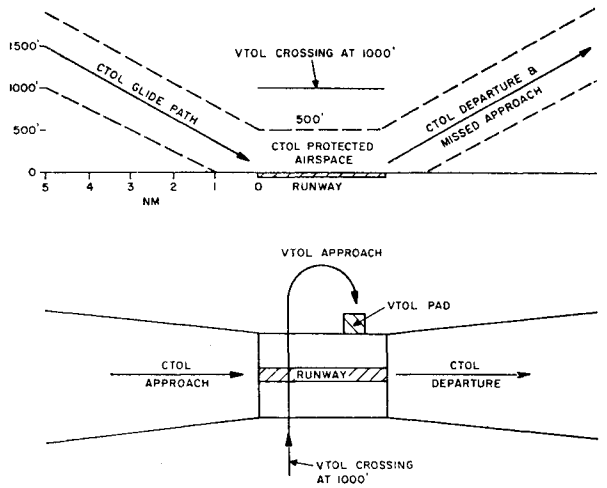

Fig. 1 Noninterfering VTOL approach to conventional airport.

presents a difficult guidance and navigation task, particularly in a wind. The steady-state turn introduces an additional integration into the control loop, making it more difficult to stabilize.

Equations of Motion

The basic dynamics of the spiral descent involve five state variables (Fig. 2):

$$\dot{\theta} = (V/r)\,[\sin(\psi-\theta) - (W/V)\sin(\eta-\theta)] \tag{1}$$

$$\dot{r} = V[\cos(\psi-\theta) - (W/V)\cos(\eta-\theta)] \tag{2}$$

$$\dot{\psi} = (g/V)\tan\phi_c \tag{3}$$

$$\dot{V} = a_c \tag{4}$$

$$\dot{h} = \dot{h}_c \tag{5}$$

It will be convenient to replace time t with turn angle θ as the independent variable in these equations. Dividing Eqs. (2-5) by Eq. (1) gives

$$\frac{dr}{d\theta} = \frac{\dot{r}}{\dot{\theta}} = r\frac{\cos(\psi-\theta) - (W/V)\cos(\eta-\theta)}{\sin(\psi-\theta) - (W/V)\sin(\eta-\theta)} \tag{6}$$

$$\frac{d\psi}{d\theta} = \frac{\dot{\psi}}{\dot{\theta}} = \frac{rg}{V^2}\frac{\tan\phi_c}{\sin(\psi-\theta) - (W/V)\sin(\eta-\theta)} \tag{7}$$

$$\frac{dV}{d\theta} = \frac{\dot{V}}{\dot{\theta}} = \frac{ra_c/V}{\sin(\psi-\theta) - (W/V)\sin(\eta-\theta)} \tag{8}$$

$$\frac{dh}{d\theta} = \frac{\dot{h}}{\dot{\theta}} = \frac{r\dot{h}_c/V}{\sin(\psi-\theta) - (W/V)\sin(\eta-\theta)} \tag{9}$$

The fifth state variable becomes time, which is defined by the reciprocal of Eq. (1):

$$\frac{dt}{d\theta} = \frac{1}{\dot{\theta}} = \frac{r/V}{\sin(\psi-\theta) - (W/V)\sin(\eta-\theta)} \tag{10}$$

One problem in specifying the nominal spiral and associated guidance parameters is determining the nominal time as a function of turn angle $t^*(\theta)$. The time to turn from θ_0 to θ_f is (Fig. 3)

$$t(\theta_f) = t(\theta_0) + \int_{\theta_0}^{\theta_f}\frac{d\theta}{\dot{\theta}} = \int_{\theta_0}^{\theta_f}\frac{r}{V_g}\,d\theta \tag{11}$$

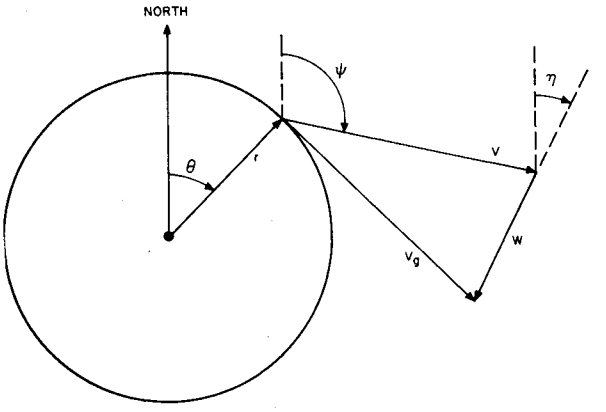

Fig. 2 Nomenclature for spiral descent.

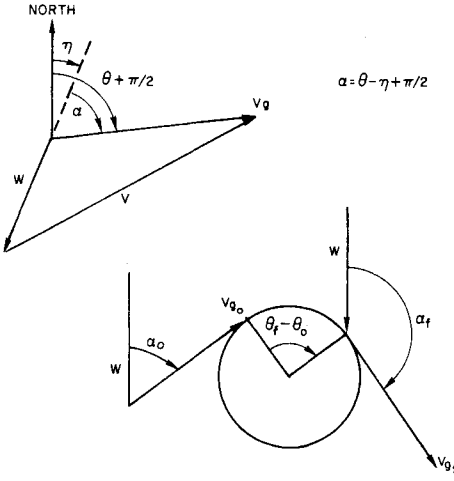

Fig. 3 Nomenclature for determining $t^*(\theta)$.

where the ground speed V_g is found by the law of cosines:

$$(V_g) = V[\sqrt{1-(W/V)^2\cos^2(\eta-\theta)} - (W/V)\sin(\eta-\theta)] \tag{12}$$

For constant spiral radius and airspeed, and defining the angle $\alpha = \theta - \eta + \pi/2$,

$$t(\theta_f) = t(\theta_0) + \frac{r}{V}\int_{\alpha_0}^{\alpha_f}\frac{d\alpha}{\sqrt{1-(W/V)^2\sin^2\alpha} - (W/V)\cos\alpha} \tag{13a}$$

$$= \frac{r}{V[1-(W/V)^2]}\,[E(W/V,\alpha) + (W/V)\sin\alpha]_{\alpha_0}^{\alpha_f} \tag{13b}$$

where $E(W/V,\alpha)$ is an elliptic integral of the second kind:

$$E\left(\frac{W}{V},\alpha\right) = \int_0^{\alpha}\sqrt{1-\left(\frac{W}{V}\right)^2\sin^2\phi}\,d\phi \tag{14}$$

The elliptic integral requires a series expansion to evaluate

$$E\left(\frac{W}{V},\alpha\right) = \alpha - \frac{1}{2}\left(\frac{W}{V}\right)^2\int_0^{\alpha}\sin^2\phi\,d\phi - \frac{(W/V)^4}{2\cdot4}\int_0^{\alpha}\sin^4\phi\,d\phi \cdots - \frac{1\cdot3\cdot5\cdots(2n-3)}{2\cdot4\cdot6\cdots2n}\left(\frac{W}{V}\right)^{2n}\int_0^{\alpha}\sin^{2n}\phi\,d\phi \tag{15}$$

where the following relation can be used:

$$\int_0^{\alpha} \sin^{2n}\phi d\phi = -\frac{\sin^{2n-1}\alpha\cos\alpha}{2n} + \frac{2n-1}{2n}\int_0^{\alpha}\sin^{2n-2}\phi d\phi \quad (16)$$

Thus, the elliptic integral can be written as

$$E\left(\frac{W}{V},\alpha\right) = \alpha - \left(\frac{W}{V}\right)^2\left(\frac{\alpha}{4} - \frac{1}{4}\sin\alpha\cos\alpha\right)$$

$$-\left(\frac{W}{V}\right)^4\left(\frac{3}{64}\alpha - \frac{3}{64}\sin\alpha\cos\alpha - \frac{1}{32}\sin^3\alpha\cos\alpha\right) + \text{HOT} \quad (17)$$

For a complete turn (i.e., $\theta_f - \theta_0 = 2\pi$),

$$E_f = 2\pi\left[1 - \frac{1}{4}\left(\frac{W}{V}\right)^2 - \frac{3}{64}\left(\frac{W}{V}\right)^4 \cdots\right] \quad (18)$$

and the time for one complete turn is

$$T = \frac{2\pi r}{V}\cdot\left[1-\left(\frac{W}{V}\right)^2\right]^{-1}\left[1 - \frac{1}{4}\left(\frac{W}{V}\right)^2 - \frac{3}{64}\left(\frac{W}{V}\right)^4\cdots\right] \quad (19)$$

Neglecting the $(W/V)^6$ term in the series expansion of E (assuming $W/V < \frac{1}{2}$) causes an error less than 0.1%, whereas neglecting the $(W/V)^4$ term causes an error less than 0.3%. However, neglecting the $(W/V)^2$ term can cause an error greater than 6%. Thus, it seems reasonable to keep terms out to $(W/V)^2$ and expect an accuracy of better than 99.7%.

Nominal Spiral Specification

The guidance concept requires the specification of the nominal state vector x^* and control vector u^* as functions of the new independent variable θ; i.e.,

$$x^*(\theta) = [r^*(\theta),\ V^*(\theta),\ \psi^*(\theta),\ t^*(\theta),\ h^*(\theta)]^T \quad (20)$$

$$u^*(\theta) = [\phi_c^*(\theta),\ a_c^*(\theta),\ \dot{h}_c^*(\theta)]^T \quad (21)$$

The basic assumptions used for the nominal spiral are constant r^*, V^*, $\dot{h}^*$, η^* and W^*.

For right-hand turns (clockwise from above), the nominal spiral state variables are defined by the following equations:

$$r^* = \text{const} \quad (22)$$

$$V^* = \text{const} \quad (23)$$

$$\psi^*(\theta) = \theta + (\pi/2) - \sin^{-1}[(W^*/V^*)\cos(\theta-\eta^*)] \quad (24)$$

$$t^*(\theta) = t^*(\theta_0) + (r^*/V^*)[1-(W^*/V^*)^2]^{-1}\{\theta-\theta_0$$

$$+ (W^*/V^*)[\cos(\theta-\eta^*) - \cos(\theta_0-\eta^*)]$$

$$-\tfrac{1}{4}(W^*/V^*)^2[\theta-\theta_0+\cos(\theta-\eta^*)\sin(\theta-\eta^*)$$

$$-\cos(\theta_0-\eta^*)\sin(\theta_0-\eta^*)]\} \quad (25)$$

$$h^*(\theta) = h^*(\theta_0) + \dot{h}^*[t^*(\theta) - t^*(\theta_0)] \quad (26)$$

where θ_0 is the entry angle into the spiral.

The nominal heading, Eq. (24), is obtained geometrically from Fig. 2. The nominal time expression uses the expansion of Eq. (17), neglecting terms of higher order than $(W/V)^2$; and inserts this into Eq. (13b). The nominal control variables for a right-hand spiral are

$$\phi_c^*(\theta) = \tan^{-1}\left\{\frac{V^{*2}}{r^* gA}\left[A + \frac{W^*}{V^*}\sin(\theta-\eta^*)\right]^2\right\} \quad (27)$$

where

$$A \triangleq \left[1-\left(\frac{W^*}{V^*}\right)^2\cos^2(\theta-\eta^*)\right]^{1/2}$$

$$a_c^* = 0 \quad (28)$$

$$\dot{h}_c^* = \frac{h^*(\theta_f) - h^*(\theta_0)}{t^*(\theta_f) - t^*(\theta_0)} = \text{const} \quad (29)$$

The nominal bank angle given by Eq. (27) is obtained by differentiating Eq. (24) with respect to θ, and substituting into Eq. (3).

For *right* turns, $\theta - \theta_0 > 0$, and Eqs. (24-29) apply. However, for *left* turns, $\theta - \theta_0 < 0$, and sign changes are required in Eqs. (24, 25, and 27).

Feedback Guidance Laws

The navigation system estimate of the vehicle state $\hat{x}(\theta)$ is compared with the nominal state $x^*(\theta)$, and any differences are fed back through the guidance gain matrix to generate corrections Δu to the nominal control $u^*(\theta)$; i.e.,

$$u(\theta) = u^*(\theta) + K[\hat{x}(\theta) - x^*(\theta)] \quad (30)$$

Theoretically, K is a 3×5 matrix, so that an error in any element of the state will produce a correction in all three control channels. In practice, however, many of the elements of K can be neglected. As a result, the guidance laws of Eq. (30) can be written for the individual control channels as follows:

$$\phi_c = \phi^*(\theta) \pm C_r(\hat{r} - r^*) + C_\psi[\hat{\psi} - \psi^*(\theta)] + C_t[\hat{t} - t^*(\theta)] \quad (31)$$

$$a_c = K_v(\hat{V} - V^*) + K_t[\hat{t} - t^*(\theta)] \quad (32)$$

$$\dot{h}_c = \dot{h}^* + K_h[\hat{h} - h^*(\theta)] \quad (33)$$

The choice of upper or lower sign in Eq. (31) depends on whether the turn is to the right or the left, respectively.

For passenger comfort and safety, the guidance commands would be limited to reasonable levels. Typical constraints might be

$$|\phi_c| < 30^\circ \quad (34a)$$

$$|a_c| < 0.1g \quad (34b)$$

$$|\dot{h}_c| < 100 \text{ ft/min} \quad (34c)$$

The gains C_t and K_t are included in Eqs. (31) and (32) to provide 4-D guidance capability. The guidance system can control time either with airspeed adjustments or by small

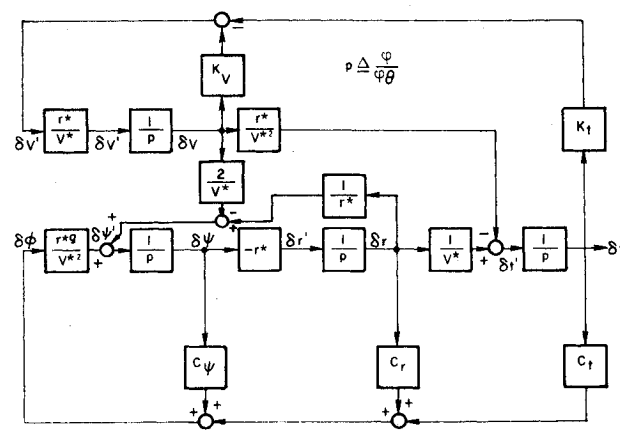

Fig. 4 Linearized block diagram of horizontal guidance system.

changes in the radius, since the time varies with both. At $V = 60$ knots and $r = 2000$ ft, a 1-knot change in airspeed has the same effect on final time as a 35-ft change in radius. Therefore, it is not desirable to control the final time with changes in radius.

Linear Analysis

The perturbation state equations for no wind, linearized about the nominal spiral, are

$$d(\delta x)/d\theta = F\delta x + G\delta u \tag{35}$$

where

$$\delta x = \begin{bmatrix} \delta r \\ \delta V \\ \delta \psi \\ \delta t \\ \delta h \end{bmatrix} \qquad F = \begin{bmatrix} 0 & 0 & -r^* & 0 & 0 \\ 0 & 0 & 0 & 0 & 0 \\ 1/r^* & -2/V^* & 0 & 0 & 0 \\ 1/V^* & -r^*/V^{*2} & 0 & 0 & 0 \\ 0 & 0 & 0 & 0 & 0 \end{bmatrix} \tag{36a}$$

$$\delta u = \begin{bmatrix} \delta a_c \\ \delta \phi_c \\ \delta h_c \end{bmatrix} \qquad G = \begin{bmatrix} 0 & 0 & 0 \\ r^*/V^* & 0 & 0 \\ 0 & gr^*/V^{*2} & 0 \\ 0 & 0 & 0 \\ 0 & 0 & r^*/V^* \end{bmatrix} \tag{36b}$$

The feedback guidance laws of Eqs. (31-33) are, in vector-matrix form,

$$\delta u = -C\delta x \tag{37}$$

where

$$-C = \begin{bmatrix} 0 & K_V & 0 & K_t & 0 \\ C_r & 0 & C_\psi & C_t & 0 \\ 0 & 0 & 0 & 0 & K_h \end{bmatrix} \tag{38}$$

A block diagram of the linearized horizontal guidance system is shown in Fig. 4. The characteristic equation for this system is given by

$$\det(I_p - F + GC) = 0 \tag{39}$$

In expanded form, this gives

$$\left[p^4 - \frac{r^*g}{V^{*2}}\left(C_\psi + \frac{V^*}{g}K_V\right)p^3 + \frac{r^{*2}g}{V^{*2}}\left(C_r + \frac{K_V C_\psi}{V^*} + \frac{K_t}{gV^*}\right)p^2 + \frac{gr^{*2}}{V^{*3}}\left(C_t - \frac{r^*}{V^{*2}}K_t C_\psi - r^* C_r K_V\right)p + \frac{gr^{*3}}{V^{*4}}\left(\frac{r^*}{V^*}C_r K_t - K_V C_t\right)\right]p - \frac{r^*}{V^*}K_h = 0 \tag{40}$$

For constant airspeed, $K_V = K_t = 0$, and the characteristic equation for the horizontal axes becomes

$$p^3 - \left(\frac{r^*g}{V^{*2}}C_\psi\right)p^2 + \left(\frac{r^{*2}g}{V^{*2}}C_r\right)p + \left(\frac{gr^{*2}}{V^{*3}}C_t\right) = 0 \tag{41}$$

For stability, the guidance gains must satisfy the following constraints:

$$C_r,\ C_t > 0 \qquad C_\psi < 0 \qquad C_t < (r^*g/V^*)C_\psi C_r$$

The linearized model of the horizontal guidance law in Fig. 4 allows application of all of the standard techniques of linear control theory to select an appropriate set of guidance gains. However, the following cautions should be noted:

1) The actual guidance law places a limit on the magnitude of the commanded bank angle.

2) The preceding analysis has neglected any attitude dynamics in the rotorcraft's response to bank-angle commands.

3) The actual system may operate outside the range where the linear model is valid.

To avoid potential problems, the linear model is used to select the guidance gains and to predict system performance; and the prediction then is verified using the nonlinear model in a trial-and-error fashion. The guidance gains C_r and C_ψ were selected iteratively from combinations that provide a natural damping of 70%. Figure 5 compares the radius error, heading error, and bank histories in response to a 100-ft initial radius error for four sets of gains. The error responses of the first three cases are very similar, whereas case 4 is extremely slow in settling out. Case 3 has a much less violent bank history and therefore was selected as the best compromise.

In Figure 5, the actual bank angle begins at the maximum allowable value (30°) for cases 1-3 in response to the initial condition error on r. To determine the effect of a finite bank angle rate, the guidance law was modified to generate a bank rate command proportional to the error between desired and actual angle, viz.,

$$\dot{\phi} = K_{\dot{\phi}}(\phi_c - \phi) \tag{42}$$

The results for $K_{\dot{\phi}} = 10\ \text{sec}^{-1}$ are compared in Fig. 6 with the infinite bank rate results of Fig. 5. The finite bank rate has little effect on the radial error history and produces only a small delay in the heading response. For lower values of $K_{\dot{\phi}}$, the response lags more but is practically the same within 40° of turn angle for $K_{\dot{\phi}} = 1.0\ \text{sec}^{-1}$.

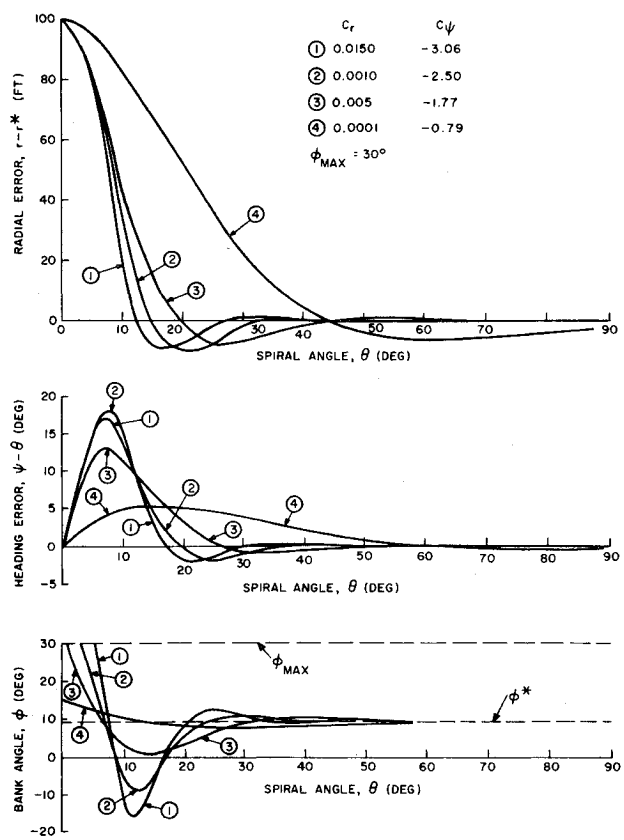

Fig. 5 Spiral guidance response for various sets of gains.

Figure 4 is also valuable for determining the sensitivity and dynamic response of the system to measurement errors. Disturbances can be entered at the points labeled $\delta\phi$, $\delta\psi$, δr, δV, and δt to correspond, respectively, to errors in the measurement of bank angle, heading angle, radial position, airspeed, and time. Since the steady-state input to all of the integrators has to be zero, the radial position error sensitivity to heading error, for example, is given by

$$\frac{\delta r}{\delta \psi} = \frac{C_{\dot{\psi}}}{C_r} \tag{43}$$

Similarly, the steady-state sensitivity of radial position error to bank angle error is given by

$$\frac{\delta r}{\delta \phi} = \frac{I}{C_r} \tag{44}$$

For the previous numerical values,

$$\frac{\delta r}{\delta \psi} = 6 \text{ ft/deg} \qquad \frac{\delta r}{\delta \phi} = 3.5 \text{ ft/deg} \tag{45}$$

Wind Estimation

A simplified wind estimator is obtained by using the off-nominal values of bank angle and heading angle to estimate the tangential and radial wind components. The changes in the north and east components are transformed from the tangential and radial components by the spiral angle θ, i.e.,

$$\begin{bmatrix} \delta \hat{W}_N \\ \delta \hat{W}_E \end{bmatrix} = \begin{bmatrix} -\sin\theta & \cos\theta \\ \cos\theta & \sin\theta \end{bmatrix} \begin{bmatrix} \delta \hat{W}_t \\ \delta \hat{W}_r \end{bmatrix} \tag{46}$$

If the rotorcraft is close to the nominal spiral, a tangential wind requires a change in bank angle, whereas a radial wind requires a change in heading into the wind. Thus, the bank and heading perturbations give an indication of the unknown wind:

$$\frac{\delta \hat{W}_t}{\delta \theta} = \frac{I}{\theta_c}\left(\frac{\partial W_t}{\partial \phi}\right)\delta\phi \tag{47}$$

$$\frac{\delta \hat{W}_r}{\delta \theta} = \frac{I}{\theta_c}\left(\frac{\partial W_r}{\partial \psi}\right)\delta\psi \tag{48}$$

where θ_c is a "characteristic turn angle" over which the wind estimate is averaged,‡ and the estimator "gains" are given by

$$\frac{\partial W_t}{\partial \phi} = \frac{r^* g}{2V^*} \quad \text{(bank sensitivity to tailwind)} \tag{49}$$

$$\frac{\partial W_r}{\partial \psi} = V^* \quad \text{(crab sensitivity to crosswind)} \tag{50}$$

The performance of the simplified estimator is shown in Figs. 7-9 for an unknown steady wind of 20 knots from four directions, using the indicated spiral parameters and $\theta_c = 90°$. The wind speed estimate is within 62% of the actual after a 90° turn in all cases, and the direction estimate is even better. The maximum radial error is less than 90 ft for initial crosswinds and less than 50 ft for an initial headwind or tailwind.

Because knowledge of the wind is crucial to the performance of the guidance law, it is important to consider the dynamics of the wind estimator. The effect of the wind estimator is to produce variations in ϕ^* and ψ^* to eliminate

‡Thus, θ_c in the "angle domain" is analagous to a characteristic response time in the conventional time domain.

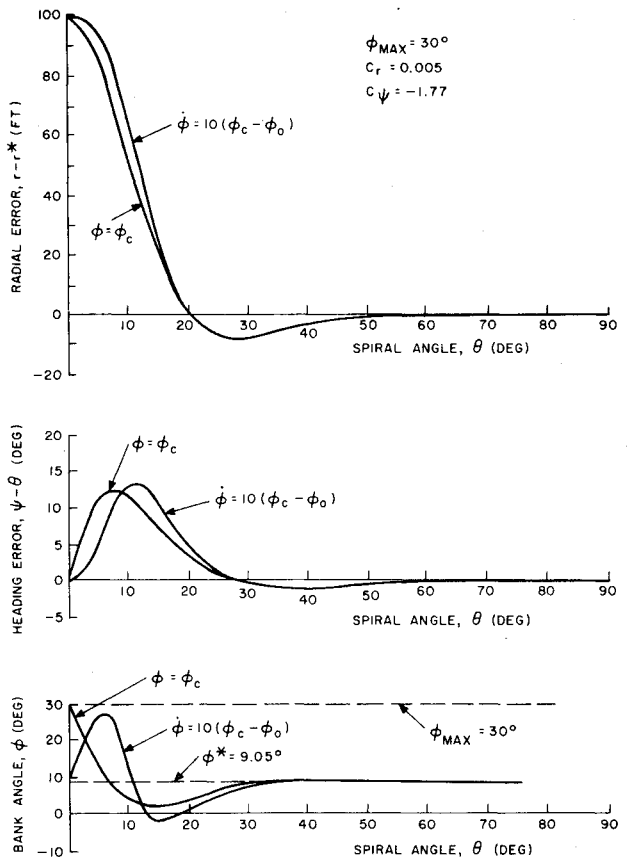

Fig. 6 Effect of finite bank rate.

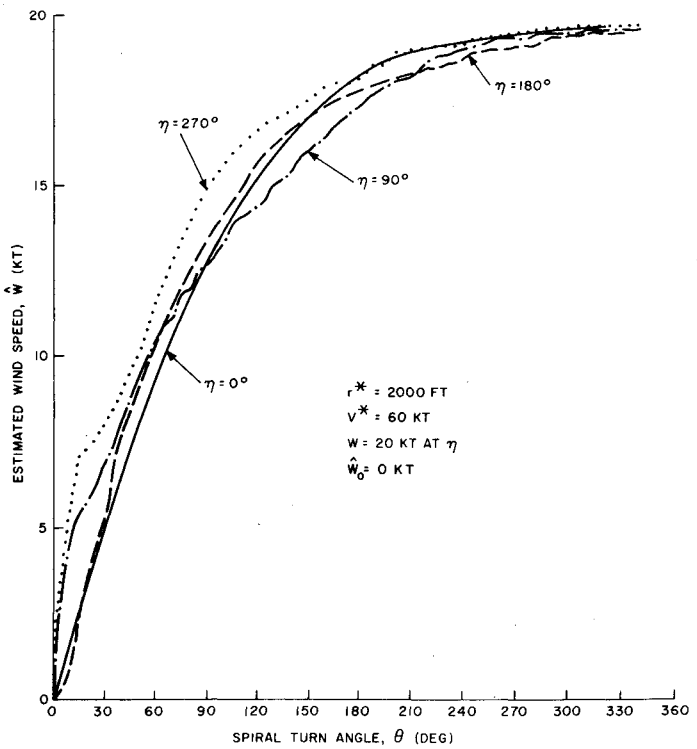

Fig. 7 Estimated wind speed with simplified estimator.

radial errors:

$$p\psi^* = (1/\theta_c)(\hat{\psi} - \psi^*) \qquad \psi_0^* = 0 \tag{51}$$

$$p\phi^* = (1/\theta_c)(\phi_c - \phi^*) \qquad \phi_0^* = \text{const} \tag{52}$$

Substituting Eqs. (51) and (52) into (31) with $C_I = 0$ and solving for ϕ gives

$$\phi_c = C_r [1 + (1/\theta_c p)] \delta r + C_\psi \psi \tag{53}$$

where $\delta r = \hat{r} - r^*$.

The result of the wind estimator is to produce an effective integral-plus-bypass term in the feedback of δr. This is exactly the technique used in mechanizing ILS couplers for conventional aircraft.

The linear signal flow diagram in the "angle domain" is shown in Fig. 10. The characteristic equation of this system is third order [cf. Eq. (41)]:

$$p^3 - C_\psi \frac{r^* g}{V^{*2}} p^2 + \frac{r^{*2} g}{V^{*2}} C_r p + C_r \frac{r^{*2} g}{V^{*2}} \frac{1}{\theta_c} = 0 \tag{54}$$

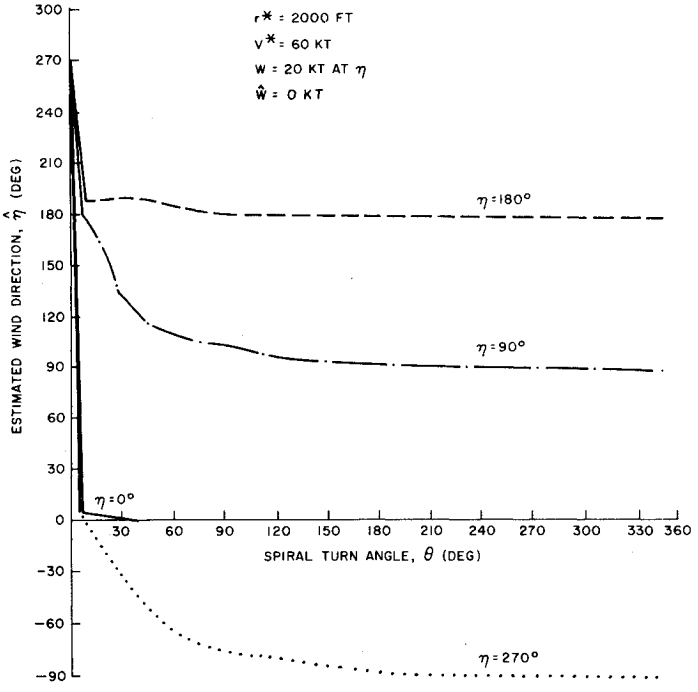

Fig. 8 Estimated wind direction with simplified estimator.

For stability, the characteristic angle of the estimator must satisfy

$$\theta_c > -(V^{*2}/r^* g C_\psi) \tag{55}$$

The sensitivity of the estimator to a crosswind is

$$\delta r \cong (-C_\psi / C_r)(W_r / V^*) \tag{56}$$

For $C_r = 0.005$, $C_\psi = -1.77$, $V^* = 60$ knots, this gives $\delta r \cong 6$ ft/knot of unknown crosswind.

The wind estimator will lag in a steady shear wind by approximately the characteristic angle θ_c. The maximum error due to a shear is about

$$\delta \hat{W} \approx \theta_c \dot{h} (V^*/r^*)(dW/dh) \delta r \tag{57}$$

Conventional automatic landing systems normally are certified on the basis of $dW/dh = 8$ knots/30 m ≈ 0.09 knot/ft. With $\theta_c = 30°$ and $\dot{h} = 500$ ft/min, this produces a maximum radial error in a shear of 38 ft. During a 300° spiral descent of 1000 ft in a steady shear of 0.01 knot/ft, the estimated wind lags the true wind, with a peak error of about 3 knots.

Guaranteed Spiral Capture

For initial spiral offsets greater than 1200-1500 ft, the spiral guidance laws will command a continuous maximum bank

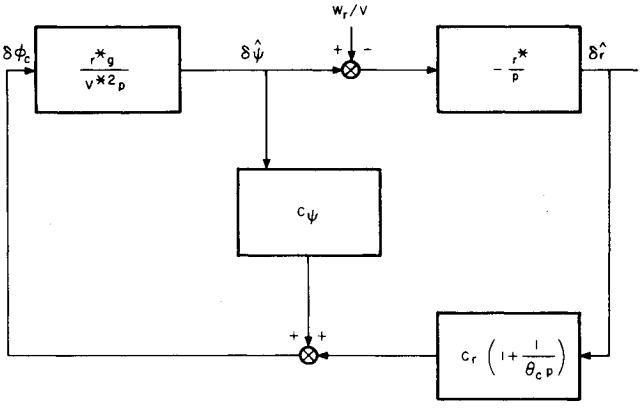

Fig. 10 Linear signal flow diagram for wind estimator.

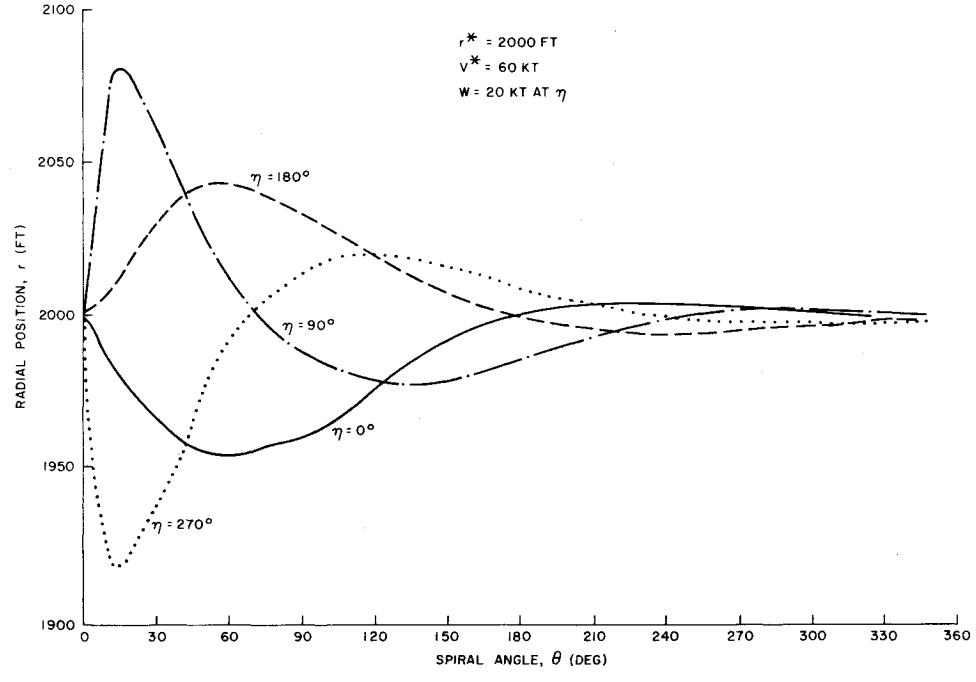

Fig. 9 Radial position accuracy with simplified wind estimator.

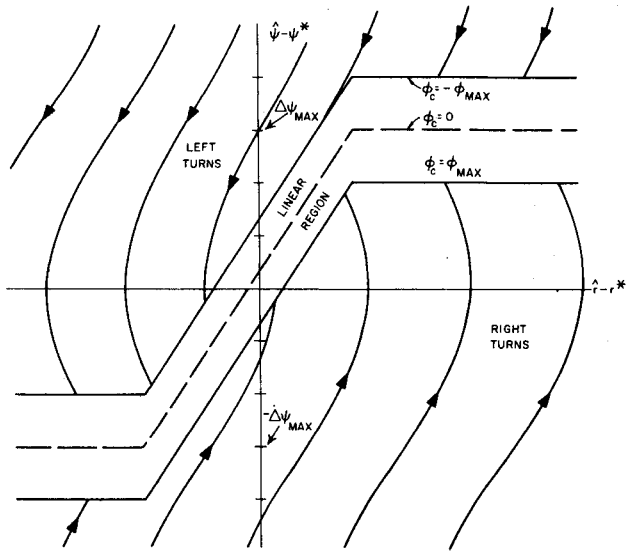

Fig. 11 Modified guidance law in phase plane.

angle (left or right) and result in a circular flight that never intercepts the desired spiral. To insure spiral capture, the guidance law can be modified to restrict the heading angle error, $\hat{\psi}-\psi^*$. The modified bank guidance algorithm for right-hand turns becomes

$$\phi_c = \begin{cases} C_\psi(\hat{\psi}-\psi^*-\Delta\psi_{max}) & (\hat{r}>r_1) \\ \phi^*+C_r(\hat{r}-r^*)+C_\psi(\hat{\psi}-\psi^*) & (r_2<\hat{r}<r_1) \\ C_\psi(\hat{\psi}-\psi^*+\Delta\psi_{max}) & (\hat{r}<r_2) \end{cases} \quad (58)$$

where

$$r_1 = r^* - \frac{C_\psi \Delta\psi_{max}+\phi^*}{C_r} \quad (59)$$

$$r_2 = r^* + \frac{C_\psi \Delta\psi_{max}-\phi^*}{C_r} \quad (60)$$

and $\Delta\psi_{max}$ is the largest value of $|\hat{\psi}-\psi^*|$ for $\phi_c=0$. Figure 11 presents the resulting phase-plane plot of the modified guidance law for a right-hand spiral.

Simulation

Two digital simulation programs have been developed for the analysis and evaluation of the spiral guidance concept. The first, containing a simple model of the vehicle dynamics and no navigation errors, was used in an interactive mode to verify the algorithms and to investigate guidance gain adjustments. The second is a modification of the VALT simulation program described in Ref. 1.

The interactive simulation numerically integrates the nonlinear equations of motion for the point-mass rotorcraft model, the finite bank angle rate command, and the wind estimator equations. The following limits are observed in the simulation:

$$|\phi_c| \le \phi_{max} \approx 30° \quad (61)$$

$$|\dot{\phi}| \le \dot{\phi}_{max} \approx 10 \text{ deg/sec} \quad (62)$$

$$|\dot{h}_c| \le \dot{h}_{max} \approx 100 \text{ ft/min} \quad (63)$$

Table 1 Results of parametric analyses

Description	Final position error, ft	Rms position error, ft	Final altitude error, ft	Rms altitude error, ft
Nominal spiral approach, 3-D	1.02	19.3	0.34	1.41
Initial crosstrack error, 1 n. mi. E	1.02	1667.7	0.34	1.40
Initial crosstrack error, 1 n. mi. W	1.05	1681.7	0.36	1.46
Initial along-track error, 1 n. mi. N	1.02	1866.2	0.34	1.37
Initial along-track error, 1 n. mi. S	1.03	2003.1	0.35	1.45
Initial ground-speed error, +20 knots	1.05	66.7	0.36	1.47
Initial ground-speed error, −20 knots	1.05	52.1	0.35	1.43
Initial altitude error, +300 ft	1.02	19.3	0.34	48.36
Initial altitude error, −300 ft	1.02	19.3	0.34	48.38
Initial track error, +30°	1.03	139.3	0.35	1.40
Initial track error, −30°	1.06	140.1	0.36	1.39
Wind speed, +15 knots	1.06	19.4	0.34	1.77
Wind speed, −15 knots	0.43	18.8	0.46	1.64
Wind direction, +90°	0.99	19.1	0.27	1.63
Wind direction, −90°	12.54	19.7	0.71	1.77
Wind speed shear, +15 knots	0.96	19.1	0.30	1.44
Wind speed shear, −15 knots	0.09	19.4	0.52	1.43
Wind direction shear, +90°	1.00	19.3	0.33	1.42
Wind direction shear, −90°	2.33	19.3	0.25	1.43
Guidance parameter, $C_r=0.001$	0.34	31.9	0.04	1.42
Guidance parameter, $C_r=0.010$	0.06	18.9	0.04	1.42
Guidance parameter, $C_\psi=-1.0$	0.06	19.8	0.04	1.42
Guidance parameter, $C_\psi=-3.0$	0.16	20.4	0.04	1.42
Guidance parameter, $K_v=-0.1$	0.11	19.7	0.04	1.39
Guidance parameter, $K_v=-0.3$	0.19	18.5	0.07	1.42
Guidance parameter, $K_h=0.5$	0.11	19.3	0.06	1.98
Guidance parameter, $K_h=2.0$	0.11	19.3	0.03	1.15
Guidance parameter, $\theta_c=45°$	0.12	19.3	0.04	1.42
Guidance parameter, $\theta_c=180°$	0.11	19.3	0.04	1.42
Guidance parameter, $W^*=30$ knots	0.34	19.1	0.32	1.15
Guidance parameter, $W^*=0$ knots	2.49	20.0	1.73	1.95
Guidance parameter, $\eta^*=180°$	2.06	20.2	0.27	2.35
Guidance parameter, $\eta^*=0°$	32.02	21.1	5.90	1.90

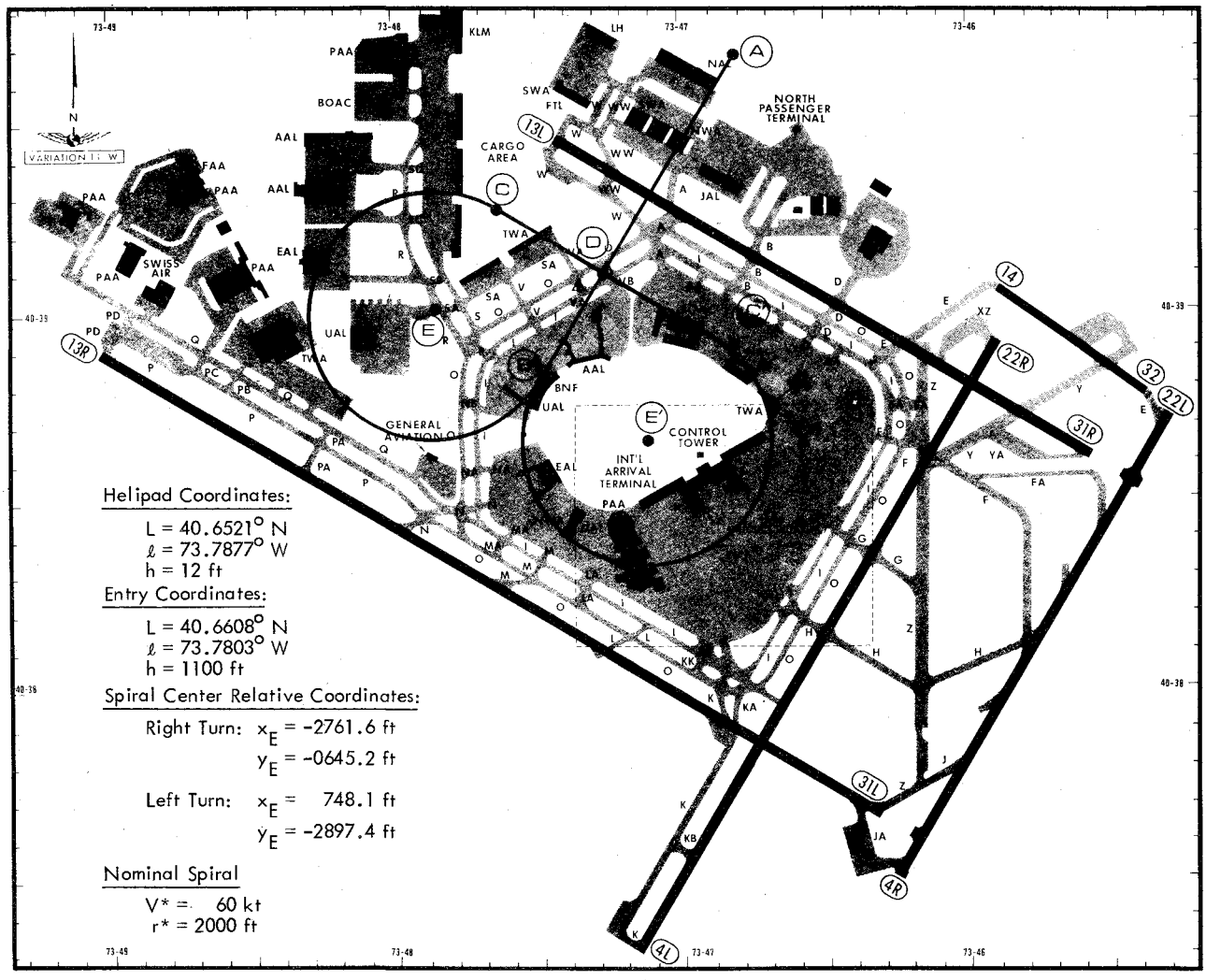

Fig. 12 Example spiral approaches to Kennedy International Airport (JFK).

Since the simplified wind estimator is based on the premise of small perturbations in ψ and ϕ from their nominal values, the wind estimates are not updated if the rotorcraft is outside an elliptical region in the center of the phase plane:

$$\left[\frac{\hat{\psi}-\psi^*}{\Delta\psi}\right]^2+\left[\frac{\hat{r}-r^*}{\Delta r}\right]^2\leq 1 \tag{64}$$

where $\Delta\psi\approx 90°$ and $\Delta r\approx 200$ ft. The estimator also is deactivated whenever the system is outside the linear bank region of the phase plane.

The interactive simulation was used to verify the algorithms for left and right spirals, for entry and exit transitions, for nominal time, for wind estimation, for guaranteed capture of the nominal, etc., as well as to select a set of satisfactory guidance gains. The resulting guidance algorithms then were implemented in the Program VALT simulation.

VALT is a nonlinear Monte Carlo simulation. First, it integrates the equations of motion which describe the response of the rotorcraft and flight control system to the guidance system commands, and it simulates the actual noisy outputs of the various navigation sensors. This part of VALT is a nonlinear, stochastic process that is intended to provide a reasonably accurate representation of the "real world." The second part of VALT simulates the operations of the onboard navigation and guidance systems.

The New York City Kennedy International Airport (JFK) was chosen as a realistic example to evaluate the performance of the spiral guidance algorithms. Figure 12 shows two example spiral approaches to an existing helipad (point D) at JFK. The entry transition (A-B) overflies the helipad at 1100 ft; a 270° descending spiral is made to the right (B-C) or left (B-C′); and a short exit transition (C-D or C′-D) completes the maneuver to hover (D). Table 1 summarizes the results of several parametric variations. Details of the guidance algorithms and additional simulation results are presented in Ref. 2.

Conclusions

The development of the spiral descent as a standard IFR approach procedure is an attractive and feasible means of satisfying several requirements for safe, efficient, and independent VTOL operations. Although the spiral descent first was conceived as a means of providing independent IFR operations for VTOL aircraft at conventional airports, the technique is equally applicable to any heliport with airspace restrictions due to other traffic, noise constraints, or obstructions.

The spiral descent retains most of the advantages of a vertical descent but requires less power and fuel, maintains forward airspeed and controllability, and avoids the vortex ring state. The effect of the wind on the spiral descent is to require a continuous variation in the rotorcraft bank angle and heading rate to remain on the desired path. The choice of maintaining constant airspeed rather than constant ground speed during the descent was made for several reasons: the descent airspeed can be selected for fuel economy; large airspeed variations could place the rotorcraft in unsafe flight regimes; and continually varying longitudinal accelerations would be necessary to maintain constant ground speed.

For 4-D guidance, the nominal time must be computed as a function of the turn angle, which requires the solution of an elliptic integral. A truncated series expansion of the elliptic integral, keeping only the first two terms, provides an accuracy of better than 0.3% in approximating the nominal time calculation.

Wind errors have a very important effect on the guidance system performance. Consequently, a wind estimator will be required for the spiral approach to adjust the nominal path appropriately. A simplified wind estimator was developed by using the off-nominal values of bank angle and heading angle to indicate errors in the tangential and radial wind components, respectively. The simplified estimator requires the specification of a characteristic angle, over which the wind estimates are averaged. In descent through a constant wind, initial errors in the estimate will be reduced to $1/e$ over the characteristic turn angle; in a constant shear, the wind estimate will lag the actual wind by approximately the characteristic angle. Simulation results have verified the performance of the simplified wind estimator.

The performance of the complete spiral guidance concept was simulated for a typical approach to New York City's Kennedy International Airport. The results have demonstrated that the spiral guidance technique is technically feasible for commercial VTOL operations.

Acknowledgment

This research was supported by NASA under Contract NAS1-12199.

References

[1]Hoffman, W. C., Hollister, W. M., and Howell, J. D., "Navigation and Guidance Requirements for Commercial VTOL Operations," NASA CR 132423; also Aerospace Systems, Inc., ASI-TR-74-17, Jan. 1974.

[2]Hoffman, W. C. and Hollister, W. M., "A Spiral Guidance Approach Concept for Commercial VTOL Operations," NASA CR 132651; also Aerospace Systems, Inc., ASI-TR-75-21, May 1975.